Extending ozone and particulate matter pollution control from New York City to Beijing

Jie Zhang[1, *], Junfeng Wang[2, *], Yele Sun[3], Jingyi Li[2], Matthew Ninneman[4], Jianhuai Ye[5], Ke Li[2], Brian Crandall[6], Jingbo Mao[7], Weiqi Xu[3], Margaret J. Schwab[1], Weijun Li[8], Xinlei Ge[2], Mindong Chen[2], Qi Ying[9], Qi Zhang[10], James J. Schwab[1,*]

[1]Atmospheric Sciences Research Center, University at Albany, State University of New York, Albany, NY 12203, USA

[2]Jiangsu Key Laboratory of Atmospheric Environment Monitoring and Pollution Control, School of Environmental Science and Engineering, Nanjing University of Information Science and Technology, Nanjing 210044, China

[3]State Key Laboratory of Atmospheric Boundary Layer Physics and Atmospheric Chemistry, Institute of Atmospheric Physics, Chinese Academy of Sciences, Beijing 100029, China

[4]School of Science, Technology, Engineering and Mathematics, University of Washington Bothell, 18115 Campus Way NE, Bothell, WA, 98011, USA

[5]School of Environmental Science & Engineering, Southern University of Science and Technology, Shenzhen 518055, China

[6]New York State Department of Environmental Conservation, NY 12233, USA

[7]Shanghai Key Laboratory of Atmospheric Particle Pollution and Prevention (LAP3), Department of Environmental Science and Engineering, Fudan University, Shanghai 200438, China

[8]Department of Atmospheric Sciences, School of Earth Sciences, Zhejiang University, Hangzhou 310027, China

[9]Department of Civil and Environmental Engineering, Texas A&M University, College Station, TX 77843, USA

[10]Department of Environmental Toxicology, University of California, Davis, Davis, CA 95616, USA

[*]To whom correspondence may be addressed. Email: jschwab@albany.edu, wangjunfengnuist@163.com, jzhang35@albany.edu

ABSTRACT

Strict emission control policies implemented in two megacities of New York City (NYC) and Beijing show impacts on the co-occurrence of their ozone (O_3) and fine particulate matter ($PM_{2.5}$) extremes. Here we show the increased O_3-$PM_{2.5}$ slope caused by the emission-related aerosol chemical composition variation in these two megacities based on the multiyear measurements, and the O_3/$PM_{2.5}$ co-occurrence is inclining to O_3 pollutions. In contrast to NYC, the O_3-$PM_{2.5}$ relationship in Beijing showed an inflection point under high $PM_{2.5}$ reflecting the O_3 formation suppression, which partially mitigated the current O_3 concentration at $PM_{2.5}$ extremes level compared to non-suppression and also contributed recent O_3 maximum enhancement in Beijing. Model simulations imply the regional equal percentage emission reductions for further pollution control to avoid any worsened O_3 pollution with the decreasing $PM_{2.5}$ extreme value and different reduction control policies are proposed for numerous Chinese main megacity clusters.

INTRODUCTION

Co-occurrence of enhanced ozone (O_3) and fine particulate matter ($PM_{2.5}$, particles with aerodynamic diameters less than 2.5 μm) concentrations adversely affects human health[1-3], and has been a wide concern in densely populated megacities [4-6]. This co-occurrence frequently happens during summer (June-August), which is due in part to stagnant meteorological conditions accompanied with high solar radiation and temperature under which high concentrations of nitrogen oxides (NO_x) and volatile organic compounds (VOCs) enhance $PM_{2.5}$ and O_3 formation[1,4].

Previous studies have demonstrated a positive relationship between the maximum daily 8-h average (MDA8) O_3 and the daily 24-h average (DA24) $PM_{2.5}$ concentrations in polluted regions during summertime[5,6]. An inflection point (IFP) in the relationship of MDA8 O_3 versus DA24 $PM_{2.5}$ was

observed at about 50~60 μg m^{-3} of DA24 $PM_{2.5}$ for Chinese megacity-clusters[6]. The MDA8 O_3 was linearly and positively correlated with DA24 $PM_{2.5}$ before the IFP while it remained relative stable despite the increasing $PM_{2.5}$ above the IFP. Such changes were mainly attributed to the scavenging of hydroperoxyl (HO_2) and/or nitrate radicals (NO_3) by high concentrations of $PM_{2.5}$ that inhibited the photochemical production of O_3[7-9].

New York City (NYC) and Beijing (BJ) are two megacities that have been extensively studied during the last two decades[10-12]. Strict emission control policies have been implemented in NYC back to 1970s with amendments in 1990 (https://www.epa.gov/clean-air-act-overview) and Beijing from 2013[13], leading to substantial decreases in $PM_{2.5}$. Compared to $PM_{2.5}$, the reduction in the O_3 maximum values were weaker in NYC[14] while with an enhancement in BJ[15-18]. This discrepancy between $PM_{2.5}$ and O_3 following the emission controls at these two locations requires further investigation. To explore these, we analyzed the relationship of MDA8 O_3 and DA24 $PM_{2.5}$ by using 19 years' measurements in NYC and 6 years' measurements in BJ and the related aerosol chemical composition measurements, compared the O_3-$PM_{2.4}$ relationship with focusing on O_3-$PM_{2.5}$ slope and their extremes concentrations (the averaged top 5% value) among their co-occurrence between NYC versus BJ with relating to the aerosol compositions variation, and explored the reasons of the current O_3 maximum enhancement in Beijing based on the IFP analysis. By comparing the successful experience in synergetic control of $PM_{2.5}$ and O_3 in NYC with that in BJ, we elucidate the potential reasons for the increased O_3-$PM_{2.5}$ slope, and highlight the future scientific strategy for controlling $PM_{2.5}$ and O_3 together in BJ and other Chinese megacity-clusters.

RESULTS

Dependence of the NYC O_3–$PM_{2.5}$ relationship on aerosol composition.

Based on the variability in DA24 $PM_{2.5}$ concentration, the 2001-2019 summertime period was separated into 4 subperiods (Fig. 1a, $SP_{NY}1$: 2001-2003, $SP_{NY}2$: 2004-2008; $SP_{NY}3$: 2009-2013, $SP_{NY}4$: 2014-2019. Fig. 1a, see **Data availability** for the data sources). The relationship between MDA8 O_3 and DA24 $PM_{2.5}$ for each subperiod was developed (Fig. 1b) following the approach in Li et al. (6) and Buysse et al. (9) As shown in Fig. 1b, the slope of MDA8 O_3 and DA24 $PM_{2.5}$ (hereafter O_3-$PM_{2.5}$ slope) increased from around 1.1 during $SP_{NY}1$ and $SP_{NY}2$ to approximately 1.7 during SP4. The MDA8 O_3 and DA24 $PM_{2.5}$ extreme concentrations decreased from 2001 to 2019 at a rate of 1.1 ppb yr^{-1} and 1.9 μg m^{-3} yr^{-1}, respectively (Fig. S1a), corresponding to a total reduction of 22% and 62% for O_3 and $PM_{2.5}$, and tracked the reductions in SO_2, VOCs, NO_x, and $PM_{2.5}$ emissions (Fig. S1b). The positive relationship of MDA8 O_3 and DA24 $PM_{2.5}$ is due in part to their common precursors, e.g., NOx and VOCs. Oxidation of O_3 precursors of NO_2 and VOCs also form nitrate and secondary organic aerosol (SOA) that are the dominant species in $PM_{2.5}$. However, the changes of other aerosol species in $PM_{2.5}$ including sulfate from oxidation of SO_2, ammonium that exists in ammonium sulfate, and primary organic aerosol (hereafter SAP), could affect the slope of O_3 versus $PM_{2.5}$. Thus, the $PM_{2.5}$ chemical compounds were divided into two groups, (1) the non-SAP compounds (e.g., SOA, nitrate and nitrate-related-ammonium) which contribute to the positive relationship of O_3 and $PM_{2.5}$, and (2) the SAP compounds, which could influence the O_3-$PM_{2.5}$ slope. A steeper slope of O_3 and $PM_{2.5}$ is expected as the SAP mass fraction in $PM_{2.5}$ decreases because more nitrate and SOA in $PM_{2.5}$ as a result of higher NOx and VOCs that are capable of producing more ozone.

To investigate this hypothesis, the measured historical PM_1 chemical composition in the NYC metropolitan area (**Method 1**) was used to track the changes in mass fractions of aerosol species. The

mass fractions of SAP decreased from 51% in 2001 to 29% in 2018 (Fig. 1c), consistent with the increased O_3-$PM_{2.5}$ slope (Fig. 1b). To test the effect of this change, $PM_{2.5}$ mass concentrations for earlier periods were adjusted downward to reflect the effective mass concentration that would have resulted if SAP of each period had equaled SAP_{ref}. Using the $SP_{NY}4$ SAP mass fraction as a reference, the aerosol mass concentration for each subperiod was adjusted using its SAP mass fraction, based on equation (1):

$$M_a = M_0 \times (1-SAP_{sp})/(1-SAP_{ref}) \quad (1)$$

where M_0 is the averaged aerosol mass concentration in each subperiod, M_a is the adjusted mass concentration, SAP_{sp} is the averaged SAP mass fraction of each subperiod ($SP_{NY}1$, $SP_{NY}2$, or $SP_{NY}3$), and SAP_{ref} is the averaged SAP mass fraction of $SP_{NY}4$. By excluding the influence of variability in SAP mass fraction, the differences of O_3-$PM_{2.5}$ slopes among the four subperiods were much smaller (Fig. 1d vs. 1b). This clearly demonstrates a fact that the reduced SAP mass fraction contributed to the increased O_3-$PM_{2.5}$ slope in NYC during the last two decades. Meanwhile, the similarity of the O_3-$PM_{2.5}$ slopes with excluded SAP fractions matched the near constant VOC/NOx emission ratio of NYC and surrounding regions (NY state as example, 1.1~1.2) in the past years as shown in following section by model simulation. While NYC experienced a reduction in MDA8 O_3 and DA24 $PM_{2.5}$ extreme value over the study period, the emissions reductions resulted relative fraction of NO_x + VOC emissions from 69% in 2001 to 85% in 2017 with more efficient ozone production per ton of total precursor emissions. The relative emission fractions dominate the O_3-$PM_{2.5}$ slopes (with higher VOC+NOx emission fraction producing a higher slope), and the overall emissions intensity controls their extremes value. The increased O_3-$PM_{2.5}$ slope highlighted the O_3/$PM_{2.5}$ co-occurrence is inclining to O_3 pollutions, and more actions for NOx and VOCs emission controls are needed for NYC regions. However, it was notable that

the 22% of the MDA8 O_3 extreme concentration was lower than the reduction of VOC emission (65% reduction) or NOx emission (66% reduction), reflecting the non-linear response of O_3 reduction to its precursors.

Increased O_3–$PM_{2.5}$ relationship in BJ.

Air quality in Beijing has been significantly improved since the clean air action in 2013, with strict emission controls mainly for SO_2 and primary particle emissions in the Beijing-Tianjin-Hebei (BTH) region (Fig. 2a) [19-20]. These emission control policies may also result in a summertime increased O_3-$PM_{2.5}$ slope as observed in NYC. To verify this, we separated the time period for BJ with existing MDA8 O_3 and DA24 $PM_{2.5}$ data (2014-2019) into two subperiods based on the $PM_{2.5}$ concentration – subperiod 1 (hereafter SP1, 2014-2016) and subperiod 2 (hereafter SP2, 2017-2019) (Fig. 2b). The DA24 $PM_{2.5}$ mass extreme concentration decreased from about 159 μg m^{-3} (SP1) to 90 μg m^{-3} (SP2) (Fig. 3), while its co-occurred O_3 extreme concentration was elevated about 3 ppb (94 ppb vs. 97 ppb), which is quite different from NYC with a 22% reduction or 20 ppb. Proposes explanations include i) the increase in the global O_3 background concentration[21,22], ii) meteorological variability[15,17,23], iii) anthropogenic emissions variation based on complex model simulations[16-19,24], iv) higher HO_2 concentrations due to the reduction of particle concentration [7], and v) the reduction of nitrogen oxides (NOx) emissions[25].

For the O_3-$PM_{2.5}$ relationship during SP1 (or SP2), in contrast to NYC, there was a lower O_3-$PM_{2.5}$ slope under high $PM_{2.5}$ concentration. By using the Community Multiscale Air Quality (CMAQ) model simulations with different scenarios, the enhanced uptake of NO_x and HO_2 by high concentrations of $PM_{2.5}$ (**Method 2**) is hypothesized to be the major cause (Fig. 2c). As the $PM_{2.5}$ concentration gets higher, greater loss of O_3 precursors (NO_x and HO_2) on aerosol surface slows down O_3 production and

reduce the O_3-$PM_{2.5}$ slope. Following the approach in Li et al.[6], an inflection point (IFP; $PM_{2.5}$ ~ 50 μg m^{-3}) was identified to separate the O_3-$PM_{2.5}$ relationship into two parts, with a linear and positive slope before the IFP (named "clean region"; Fig. 3) and relatively slower ozone increasing followed $PM_{2.5}$ enhancement after the IFP (named "polluted region"). Clearly, the O_3/$PM_{2.5}$ co-occurrence of NYC located in the clean regions, with a simple linear O_3-$PM_{2.5}$ relationship.

Comparing the O_3-$PM_{2.5}$ relationship of Beijing between SP1 vs. SP2, consistent with the NYC pattern, the O_3-$PM_{2.5}$ slope before the IFP increased from SP1 to SP2 , and the O_3-$PM_{2.5}$ slopes in SP1 and SP2 were similar after adjusting for the variability of SAP mass fraction (Fig. 2d, Fig. S2 and **Method 1** for the aerosol composition mass fraction). The enhanced (VOCs+NOx) emission fraction due to the control policies of SP2 are the dominant reason for the increased O_3-$PM_{2.5}$ slopes, in spite of the increase in temperature from SP1 to SP2 (Fig. S3)[15,26]. Meanwhile, the near-constant VOC/NOx emission ratio of BJ (about 1.0, Fig. 2a) in the six years also promotes the similarity of the modified O_3-$PM_{2.5}$ slopes as shown in following section by model simulation. Considering BJ extreme air pollution episodes being influenced by regional transport from BTH[27], the increased O_3-$PM_{2.5}$ slope in BJ represents a regional phenomenon in the BTH region (Fig. 2e) and reflects variability in the current regional emission abatements with greater SO_2 and $PM_{2.5}$ reduction.

Following the increased O_3-$PM_{2.5}$ slope before the IFP in SP2, the O_3 concentration kept higher at the same $PM_{2.5}$ level in SP2 comparing to SP1 after IFP. However, the O_3 suppression by the high $PM_{2.5}$ mass concentration shallowed the O_3-$PM_{2.5}$ slope after SPF, which partly mitigated the current potential O_3 increase at the SP2 $PM_{2.5}$ extremes level (90 μg m^{-3}). Based on the O_3-$PM_{2.5}$ relationship before IFP of SP2, the O_3 concentration at 90 μg m^{-3} was estimated to be as high as 146 ppb, which roughly implied a 34% benefit from the O_3 suppression under this $PM_{2.5}$ level considering the current O_3 extreme of 97

ppb. It is expected that if the VOC and NOx emissions of BTH keep constant in further, lower $PM_{2.5}$ extremes level caused by the SO_2/or primary $PM_{2.5}$ reduction would decline the O_3 production suppression and result more severe O_3 extremes. This kind of O_3 enhancement will also happen if the VOC and NOx emission reduction is not enough to make up the O_3 enhancement due to the declined O_3 production suppression, which matched the enhanced O_3 concentration (3 ppb) under the $PM_{2.5}$ extreme value dropped from higher one of SP1 (159 μg m^{-3}) to lower one of SP2 (90 μg m^{-3}) with the slightly change of VOC and NOx emission from SP1 to SP2 (Fig. 2a). Moreover, Fig. 3 demonstrates that if SAP concentrations decrease to near zero in BJ as a limiting case, O_3 concentrations (purple arrow) and the O_3-$PM_{2.5}$ slope (blue shaded region) will likely increase, as shown in the CMAQ simulation with only SO_2 emission abatement (Fig. 2c).

Regional equal percentage emission reductions.

To avoid further worsened O_3 pollution with the decreasing $PM_{2.5}$ extremes, regional equal percentage emission reductions in VOCs, NO_x, SO_2 and $PM_{2.5}$ is suggested by the CMAQ simulations (Fig. 2f and Fig. S4) as an achievable way. However, the effect of such emission policies on ozone extremes will not be significant until $PM_{2.5}$ below to the IFP and Beijing stepping into the "clean region" where current NYC locates. Under regional equal percentage emission reductions, the O_3-$PM_{2.5}$ relationship of Beijing before IFP would keep constant (Fig. 2f). Furthermore, the required BTH regional emission reductions based on the 2019 annual emissions were about 29%, 42%, 53% and 70% (**Method 3**), respectively, in order to reach the BJ $PM_{2.5}$ concentration equal to the IFP (50 μg m^{-3}, hereafter "Goal 1"), the 2001 NYC top5% DA24 $PM_{2.5}$ concentration level (39 μg m^{-3}, hereafter "Goal 2"), the MDA8 O_3 concentration below China's O_3 standards (75 ppb, which was related to DA24 $PM_{2.5}$ about 29 μg m^{-3}

for Beijing, hereafter "Goal 3") and the 2019 NYC DA24 $PM_{2.5}$ concentration extreme concentration (15 μg m^{-3}, hereafter "Goal 4") (Fig. 3).

The emission related O_3-$PM_{2.5}$ slope variations were also observed in other megacity clusters, such as Yangtze River Delta (YRD) and Pearl River Delta (PRD) (Fig. 4 and S5). The O_3-$PM_{2.5}$ slope of YRD increased in recent years (Fig. 4a), consistent with the larger reductions in SO_2 and primary $PM_{2.5}$ than non-SAP species (Fig. 4b). For example, to reach the above four goals in Shanghai, the emissions in YRD need to be reduced by 13%, 28%, 32% and 59%, respectively on the basis of 2019 annual emissions (**Method 3**). Comparatively, the O_3-$PM_{2.5}$ slope of PRD was only slightly increased (Fig. 4c), due to the small changes in emission ratios of SO_2 and $PM_{2.5}$ (Fig. 4d). Meanwhile, the maximum DA24 $PM_{2.5}$ concentration of PRD in SP2 was below IFP, and further emission reductions would cause effective reductions in the co-occurrence of O_3 and $PM_{2.5}$. The DA24 $PM_{2.5}$ extreme concentration in Guangzhou (the representative of PRD) in 2019 was 36.2 μg m^{-3}, which was already below IFP and 2001 NYC top5% DA24 $PM_{2.5}$ concentration level. However, additional regional and synchronous emission reductions in PRD by 14% and 69% (**Method 3**), respectively are needed to meet the other two goals ("Goal 3 and 4").

DISCUSSION

Under current emission policies for NYC and BJ with larger reductions in the emissions of SO_2 and $PM_{2.5}$ than those of VOCs and NO_x, we obtained an increased O_3-$PM_{2.5}$ slope ("worsened O_3 at same $PM_{2.5}$ level") and expected the continually inclining of the O_3/$PM_{2.5}$ co-occurrence to O_3 pollutions in the further if the same policies lasting. However, Beijing will suffer more complicated conditions than NYC, as the O_3 production suppression under the high $PM_{2.5}$ level which shallowed the O_3-$PM_{2.5}$ slope after the IFP. This ozone formation suppression in Beijing partly mitigated the current O_3 enhancement

at the SP2 $PM_{2.5}$ extremes level comparing to the originally O_3 concentration without any suppression. If the VOCs and NOx emissions in BTH did not decrease enough to make up the enhanced O_3 from the declined O_3 production suppression under the decreased $PM_{2.5}$ concentration, more worsen O_3 extremes pollutions may occur. To avoid further worsened O_3 pollution at the same $PM_{2.5}$ level, we suggest reducing $PM_{2.5}$ to the IFP and below following an average regional equal percentage emission reduction of 29% in BTH, with other different emission controls are needed for other regions.

It is notable that this study simply assumed different linear relationships before and after IFP to predigest the O_3-$PM_{2.5}$ relationship, while there may be more complex non-linear relationships (Fig. S6 as the example), and IFP could represent one approximate and its location could be related with NOx and HO_2 uptake parameters, such as aerosol surface, uptake efficiencies, etc. Notably, the observations at YRD and PRD showed a negative correlation between O_3 and $PM_{2.5}$ at $PM_{2.5}$ > about 70 μg m^{-3} (Fig. 4a and 4c), matching the enhanced O_3 suppression and implying the complex non-linear O_3-$PM_{2.5}$ relationship. Though further studies are warranted to verify the non-linear relationships, this study provided a straightforward prospective to understanding the co-occurrences of O_3 and $PM_{2.5}$ in densely populated megacities during the summer heat days and their responds to the emission policies. We used NYC and Beijing as the examples for the comparison as they represent different emission stages with NYC (current at "clean region", Fig. 3) more likely being the further of Beijing (current at "polluted region", Fig. 3). As the heat days occurring more often, the emission policy related O_3/$PM_{2.5}$ co-occurrences worth to be studied in a worldwide, with focusing on their further variation trends (O_3-$PM_{2.5}$ slope and extreme concentrations) and the interplay between O_3 and $PM_{2.5}$ in order to avoid the ozone worsen under emission controls, especially for the cities with $PM_{2.5}$ extreme concentrations above the inflection point.

METHODS

M1. Aerosol chemical composition measurements.

The Aerodyne Aerosol Mass Spectrometer (AMS) was deployed during the field campaign to obtain the chemical composition of non-refractory particulate matter smaller than 1 μm in diameter (NR-PM_1). In this study, we assumed that the aerosol composition of PM_1 is similar to $PM_{2.5}$ based on (1) the current application of AMS for PM_1 and $PM_{2.5}$ chemical composition measurements in Beijing with a similar mass fraction[28] and (2) the domination contribution (>70%) of PM_1 to $PM_{2.5}$ in NYC[29,30] with similar contribution (around 0.7) from each main composition (e.g. sulfate, nitrate, ammonium) of PM_1 to $PM_{2.5}$ comparing the measurements from an AMS to by a Particle-into-Liquid Sampler (PILS) coupled with two Metrohm Compact 761 Ion Chromatography (IC) systems (PILS-IC)[29]. Also, we ignored primary black carbon due to the limitation of AMS. For NYC, AMS field measurements were made during the summers of 2001[31], 2009[27,32], 2011[33], and 2018[10,30] in NYC or the surrounding area. The aerosol mass fractions of (1) 2001 measurements were used for the subperiod of 2001-2003, (2) the average of 2001 and 2009 for subperiod of 2004-2008, (3) 2011 for subperiod of 2009-2013, and (4) 2018 for subperiod of 2014-2019. For BJ, AMS measurements were made at the tower branch of the Institute of Atmospheric Physics, a typical urban site located between the north 3rd and 4th ring road in Beijing[34] during 06/07-07/08 in 2014 and 06/01-06/29 in 2017, which were used for subperiod of 2014-2016 and 2017-2019, respectively. The measured OA organic mass spectra have been applied by the Positive Matrix Factorization (PMF) analysis to separate into different OA factors/subtypes[35], such as the oxidized organic aerosols (OOAs) as a surrogate of SOA, and the hydrocarbon-like OA (HOA) as a surrogate of POA[36,37].

M2. Community Multiscale Air Quality Model (CMAQ). The Community Multiscale Air Quality

Model (CMAQ) version 5.2 was applied in the current study, coupled with SAPRC-07 mechanism and updated AERO6 aerosol module. The updates including the heterogeneous loss of NO_2, SO_2, glyoxal, and methylglyoxal to form nitrate, sulfate, and SOA. The reactive surface uptake coefficient of NO_2, glyoxal, and methylglyoxal followed Ying et al. (2014)[38] and Ying et al. (2015)[39], respectively and the heterogeneous formation of sulfate from surface-controlled reactive uptake of SO_2 followed Hu et al (2016)[40]. In addition, the uptake of HO_2 onto aerosol surfaces was considered by following Xue et al. (2014)[41] with an uptake coefficient (γ_{HO2}) of 0.2[7]. The model was applied to simulate O_3 and $PM_{2.5}$ formation during June-August 2017 using a 36 km × 36 km horizontal domain that covers China and surrounding countries in East Asia. The meteorological fields were generated by the Weather Research and Forecasting WRF (v4.0.) with a 3D nudging of winds, temperature, and water vapor above the PBL based on the NCEP ADP Global Upper Air Observational Weather Data (https://rda.ucar.edu/datasets/ds351.0/#!access). For anthropogenic emissions, the monthly Multi-resolution Emission Inventory for China (MEICv1.3, http://www.meicmodel.org) and the Regional Emission inventory in Asia (REASv3.1, https://www.nies.go.jp/REAS/) were applied to China and the rest part of the domain, respectively. The resolution of both inventories was 0.25°x0.25°. Biogenic emissions were generated by the Model for Emissions of Gases and Aerosols from Nature (MEGAN) v2.1, with the leaf area index (LAI) from the 8-day Moderate Resolution Imaging Spectroradiometer (MODIS) LAI product (MOD15A2) and the plant function types (PFTs) from the Global Community Land Model (CLM 3.0). Open burning emissions were based on the Fire Inventory from NCAR (FINN). Dust and sea salt emissions were generated via inline processing during CMAQ simulations. Lightning-induced NO_x production was not included in the current study. Initial and boundary conditions were based on the default vertical distribution of concentrations provided by CMAQ that represent a clean continental condition with a fixed background O_3 concentration ranges from 30 to 70 ppb. The first three

days were taken as spin-up days and results were excluded from the analysis. The comparison between the CMAQ simulation with the observations for the 24 cities in the BTH and its nearby region (Fig. S6) was shown in Fig. S7-S9. In general, the model can well capture the temporal variations of both O_3 and $PM_{2.5}$ in all the cities, with the performance statistics conformed to the recommend benchmarks by Emery et al. (2017)[42] as shown in Table S1. Besides the base case with the default emissions of 2016, other cases were designed to represent the possible changes of anthropogenic emissions in the future, including (1) proportional reductions in all the anthropogenic sectors by 25%, 50%, and 75%, respectively, and (2) reductions in SO_2 and primary particulate matter by 50% and 100%, respectively. The CMAQ simulation results are available from the corresponding authors on request.

M3. Synchronous emission reductions estimation. The relationship of top5% DA24 $PM_{2.5}$ concentration with an emission reduction ratio of Beijing (71.6 μg m^{-3}/100% MEIC reduction, Fig. S10a) and other cities (75.4 μg m^{-3}/100% MEIC reduction for Shanghai and 34.3 μg m^{-3}/100% MEIC reduction for Guangzhou, Fig. S10b and S10c) from the model simulation was used to estimate the synchronous emission abatements. Meanwhile, the ratios of observed top5% DA24 $PM_{2.5}$ to the simulated one (1.2 for Beijing, 1.0 for Shanghai, and 0.9 for Guangzhou) were used to correct the above relations, assuming they were the simulation uncertainty. The corrected relations were 85.9 μg m^{-3}/100% MEIC reduction for Beijing, 75.4 μg m^{-3}/100% MEIC reduction for Shanghai, and 30.9 μg m^{-3}/100% MEIC reduction for Guangzhou, respectively. The observed 2019 top5% DA24 $PM_{2.5}$ concentration of Beijing (74.8 μg m^{-3}), Shanghai (59.8 μg m^{-3}) and Guangzhou (36.2 μg m^{-3}) were used as the references. The MDA8 O_3 concentration below China's O_3 standards (about 75ppb) related DA $PM_{2.5}$ concentration for Beijing (about 29 μg m^{-3}), Shanghai (about 36 μg m^{-3}), and Guangzhou (about 32 μg m^{-3}) were estimated based on the O_3-$PM_{2.5}$ relations from Fig. 3 and 4a and 4c.

DATA AVAILABILITY

MDA8 O_3, DA24 $PM_{2.5}$ concentration, and pollutants emission inventory sources. Summertime (June-August) 2001-2019, MDA8 O_3 concentrations, and DA24 $PM_{2.5}$ concentrations for the Queens College site were obtained from https://www.epa.gov/outdoor-air-quality-data/download-daily-data. The MDA8 O_3 and daily average $PM_{2.5}$ concentration for summer (June-August) 2014-2019 for BJ were obtained from the Chinese Ministry of Ecology and Environment (MEE) website (http://english.mee.gov.cn/). The VOC, NO_X, SO_2 and $PM_{2.5}$ annual emission rates for NYC and NY state were obtained from the EPA National Emissions Inventory website (https://www.epa.gov/air-emissions-inventories/national-emissions-inventory-nei). The AMS measured aerosol chemical composition data for (1) 2001, 2009, and 2011 NYC field campaigns can be found at https://sites.google.com/site/amsglobaldatabase/, (2) the 2018 NYC field campaign data can be found at https://www-air.larc.nasa.gov/missions/listos/index.html.

ACKNOWLEDGEMENT

The authors acknowledge support from the New York State Energy Research and Development Authority (NYSERDA, no. 48971), the National Natural Science Foundation of China (no. 42021004), the National Key Research and Development Program of China (no. 2018YFC0213802). We acknowledge the free use of ozone and $PM_{2.5}$ data from the US EPA and China's Ministry of Ecology and Environment. Special thanks to Prof. Daniel J. Jacob from Harvard University for providing valuable comments for this study.

AUTHOR CONTRIBUTIONS

J.Z., J.W. and J.S. designed the research and led the writing, J.Z., Y.S., and W.X. performed

experiments, J.L. performed the CMAQ model simulation, J.Z., J.W., Y.S. and J.L. analyzed the data, M.N., J.Y., K.L., B.C., J. M., M.S., W.L., X.G., M.C., Y.Q., and Q.Z. contributed significant comments and editing of the paper.

COMPETING INTERESTS

The authors declare no competing interests.

References

1. Schnell, J. L. & Prather, M. J. Co-occurrence of extremes in surface ozone, particulate matter, and temperature over eastern North America. *Proc. Natl Acad. Sci. USA* 114, 2854–2859 (2017).
2. Dear, K., Ranmuthugala, G., Kjellstrom, T., Skinner, C. & Hanigan, I. Effects of temperature and ozone on daily mortality during the August 2003 heat wave in France. *Arch. Environ. Occup. Health* 60(4), 205–212 (2005).
3. Willers, S. M. et al. High-resolution exposure modelling of heat and air pollution and the impact on mortality. *Environ Int* 89,102–109 (2016).
4. Zhao, K. et al. A high resolution modeling study of a heat wave-driven ozone exceedance event in New York City and surrounding regions. *Atmos. Environ.* 199, 368–379 (2019).
5. Zhu, J., Chen, L., Liao, H. & Dang, R. Correlations between $PM_{2.5}$ and ozone over China and associated underlying reasons. *Atmosphere* 10, 352 (2019).
6. Li, K. et al. A two-pollutant strategy for improving ozone and particulate air quality in China. *Nat. Geosci*. 12, 906–910 (2019).
7. Li, K. et al. Anthropogenic drivers of 2013–2017 trends in summer surface ozone in China. *Proc. Natl Acad. Sci. USA* 116, 422–427 (2019).
8. Jacob, D. J. Heterogeneous chemistry and tropospheric ozone. *Atmos. Environ.* 34, 2131–2159 (2000).
9. Buysse, C. E., Kaulfus, A., Nair, U. & Jaffe, D. A. Relationships between Particulate Matter, Ozone, and Nitrogen Oxides during Urban Smoke Events in the Western US. *Environ. Sci. Technol.* 53, 12519−12528 (2019).
10. Zhang, J. et al. Mobile Laboratory Measurements of High Surface Ozone Levels and Spatial Heterogeneity During LISTOS 2018: Evidence for Sea Breeze Influence. *J. Geophys. Res. Atmos.*

124, 1-12 (2020).

11. Sun, Y. et al. Investigation of the sources and evolution processes of severe haze pollution in Beijing in January 2013. *J. Geophys. Res. Atmos.* 119, 4380-4398 (2014).
12. Wang, J. et al. Fast sulfate formation from oxidation of SO_2 by NO_2 and HONO observed in Beijing haze. *Nat. Commun.* 11, 2844 (2020)
13. Zhang, Q. et al. Drivers of improved $PM_{2.5}$ air quality in China from 2013 to 2017. *Proc. Natl. Acad. Sci. USA*, 116, 24463–24469 (2019).
14. Blanchard, C. L., Shaw, S. L., Edgerton, E. S., & Schwab, J. J. Emission influences on air pollutant concentrations in New York State: I. ozone. *Atmos. Environ.:X* 3, 100033 (2019).
15. Liu, Y., & Wang, T. Worsening urban ozone pollution in China from 2013 to 2017 – Part 1: The complex and varying roles of meteorology. *Atmos. Chem. Phys*. 20, 6305–6321 (2020).
16. Liu, Y., & Wang, T. Worsening urban ozone pollution in China from 2013 to 2017 – Part 2: The effects of emission changes and implications for multi-pollutant control. *Atmos. Chem. Phys*. 20, 6323–6337 (2020).
17. Li, K. et al. Increases in surface ozone pollution in China from 2013 to 2019: anthropogenic and meteorological influences, *Atmos. Chem. Phys.* 20, 11423–11433 (2020).
18. Wang, Y. et al. Contrasting trends of $PM_{2.5}$ and surface-ozone concentrations in China from 2013 to 2017. *Natl. Sci. Rev.*, 7(8), 1331–1339 (2020).
19. Cheng, J. et al. Dominant role of emission reduction in $PM_{2.5}$ air quality improvement in Beijing during 2013–2017: a model-based decomposition analysis. *Atmos. Chem. Phys.* 19, 6125–6146 (2019)
20. Wang, S. W. et al. Natural gas shortages during the "coal-to-gas" transition in China have caused a large redistribution of air pollution in winter 2017. *Proc. Natl. Acad. Sci. USA* 117 (49), 31018-

31025 (2020).

21. Yeung, L. Y. et al. Isotopic constraint on the twentieth-century increase in tropospheric ozone. *Nature* 570, 224−227 (2019).

22. Tan, Z. et al. No Evidence for a Significant Impact of Heterogeneous Chemistry on Radical Concentrations in the North China Plain in Summer 2014. *Environ. Sci. Technol. Lett*. 54, 10, 5973–5979 (2020).

23. Zhao, S. et al. $PM_{2.5}$ and O_3 pollution during 2015-2019 over 367 Chinese cities: Spatiotemporal variations, meteorological and topographical impacts. *Environ. Pollut.* 64, 114694 (2020).

24. Chu, B. et al. Air pollutant correlations in China: secondary air pollutant responses to NOx and SO_2 control. *Environ. Sci. Technol. Lett*. 7, 10, 695–700 (2020).

25. Chen, X. et al. Chinese regulations are working - why is surface ozone over industrialized areas still high? Applying lessons from Northeast US air quality evolution. *Geophys. Res. Lett.* e2021GL092816 (2021).

26. Shi, Z. et al. Sensitivity analysis of the surface ozone and fine particulate matter to meteorological parameters in China. *Atmos. Chem. Phys.* 20, 13455–13466 (2020).

27. Chang, X. et al. Contributions of inter-city and regional transport to $PM_{2.5}$ concentrations in the Beijing-Tianjin-Hebei region and its implications on regional joint air pollution control. *Sci. Total Environ.* 660, 1191-1200 (2019).

28. Sun, Y. L. et al. Chemical differences between PM_1 and $PM_{2.5}$ in highly polluted environment and implications in air pollution studies. *Geophys. Res. Lett.* 47, e2019GL086288 (2020).

29. Sun, Y. L. et al. Characterization of the sources and processes of organic and inorganic aerosols in New York city with a high-resolution time-of-flight aerosol mass spectrometer. *Atmos. Chem. Phys.* 11, 1581–1602 (2011).

30. Zhang, J. et al. Long Island enhanced aerosol event during 2018 LISTOS: Association with heatwave and marine influences. *Environ. Pollut.* 270, 116299 (2021).
31. Drewnick, F. et al. Measurement of ambient aerosol composition during the PMTACS-NY 2001 using an aerosol mass spectrometer. Part ii: Chemically speciated mass distributions. *Aerosol Sci. Technol.* 38, 104-117 (2004).
32. Sun, Y. L. et al. Factor Analysis of Combined Organic and Inorganic Aerosol Mass Spectra from High Resolution Aerosol Mass Spectrometer Measurements. *Atmos. Chem. Phys*. 12, 8537-8551 (2012).
33. Zhou, S. et al. Influences of upwind emission sources and atmospheric processing on aerosol chemistry and properties at a rural location in the Northeastern US. *J. Geophys. Res. Amos.* 121, 6049–6065 (2016).
34. Sun, Y. L. et al. Characterization of summer organic and inorganic aerosols in Beijing, China with an Aerosol Chemical Speciation Monitor. *Atmos. Environ.* 51, 250–259 (2012).
35. Ulbrich, I. M. et al. Interpretation of organic components from Positive Matrix Factorization of aerosol mass spectrometric data. *Atmos. Chem. Phys*. 9, 2891-2918 (2009).
36. Ng, N. L. et al. Organic aerosol components observed in Northern Hemispheric datasets from Aerosol Mass Spectrometry. *Atmos. Chem. Phys*. 10, 4625-4641 (2010).
37. Zhang, Q. et al. Understanding atmospheric organic aerosols via factor analysis of aerosol mass spectrometry: a review. *Anal. Bioanal. Chem.* 401(10), 3045-3067 (2011).
38. Ying, et al. Impacts of Stabilized Criegee Intermediates, surface uptake processes and higher aromatic secondary organic aerosol yields on predicted $PM_{2.5}$ concentrations in the Mexico City Metropolitan Zone. *Atmos. Environ.* 94, 438-447 (2014).
39. Ying, Q., Li, J. & Kota, S. H. Significant Contributions of Isoprene to Summertime Secondary

406 Organic Aerosol in Eastern United States. *Environ. Sci. Technol.* 49, 13, 7834–7842 (2015).
407 40. Hu, J., Chen, J., Ying, Q. & Zhang, H. One-Year Simulation of Ozone and Particulate Matter in
408 China Using WRF/CMAQ Modeling System. *Atmos. Chem. Phys.* 16, 10333–10350 (2016).
409 41. Xue, L. K. et al. Ground-level ozone in four Chinese cities: precursors, regional transport and
410 heterogeneous processes. *Atmos. Chem. Phys.* 14, 13175–13188 (2014).
411 42. Emery, C. et al. Recommendations on statistics and benchmarks to assess photochemical model
412 performance. *J. Air Waste Manag. Assoc.* 67, (5), 582-598 (2017).

Figure legends

Figure 1. O_3 and $PM_{2.5}$ in NYC. a, The time series of the average DA24 $PM_{2.5}$ and top5% DA24 $PM_{2.5}$ mass concentrations in NYC for each subperiod specified in the main text (the dashed boxes indicate the four subperiods with subperiod 1 ($SP_{NY}1$): 2001-2003, subperiod 2 ($SP_{NY}2$): 2004-2008, subperiod 3 ($SP_{NY}3$): 2009-2013, subperiod 4 ($SP_{NY}4$): 2014-2019); **b,** NYC O_3-$PM_{2.5}$ relationship for the different subperiods (Colored by SAP mass fraction. The DA24 $PM_{2.5}$ data were binned in increments of 5 μg m^{-3}. The shaded area indicates 25%-75% data range of each bin. The O_3 concentration of each point was obtained by averaging the 25%-75% data. All p-value < 0.01); **c,** The aerosol mass fraction for each subperiod in NYC based on the AMS measurement from the representative year (2001 for $SP_{NY}1$, the average of 2001 and 2009 for $SP_{NY}2$, 2011 for $SP_{NY}3$ and 2018 for $SP_{NY}4$. Black dash box indicates non-SAP compounds, including SOA, nitrate and nitrate-related-ammonia); **d,** Adjusted O_3-$PM_{2.5}$ relationship when removing the influence of variability in SAP (* means adjusted value. All p-value < 0.01).

Figure 2. O_3 and $PM_{2.5}$, and related emissions in BJ and BTH. a, The 2014 and 2016 MEIC anthropogenic emissions in BTH (including provinces of Beijing, Tianjin and Hebei) (Note: 2016 MEIC anthropogenic emissions was used for 2017 summertime simulation and also for showing the emission variation trend); b, The time series of the average DA24 $PM_{2.5}$ and top5% DA24 $PM_{2.5}$ mass concentrations (the dash boxes indicate the two subperiods with subperiod 1 (SP1): 2014-2016, subperiod 2 (SP2): 2017-2019) ; c, The O_3 vs $PM_{2.5}$ relationship for observations, CMAQ simulations with only NOx uptake, CMAQ simulations with NOx and HO_2 uptake, and 50% abatements of SO_2 emissions for 2017; d, The O_3-$PM_{2.5}$ relationship of BJ for SP1 and SP2, and the adjusted O_3-$PM_{2.5}$ relationship based on the mass fraction in (c) (denoted by * in the legend, the $PM_{2.5}$ data were binned in increments of 5 μg m^{-3}) ; e, The O_3 vs $PM_{2.5}$ relationship of main urban cities in BTH for subperiod 1 and subperiod 2 (including Beijing, Tianjin, Shijiazhuang, Tangshan and Baoding, and the locations were shown in Figure S6. The error bar indicates 25-75% data range); f, The O_3 vs $PM_{2.5}$ relationship for different simultaneous emission abatement scenarios based on CMAQ simulations with NOx and HO_2 uptake for 2017.

Figure 3. Diagram of the current and future O_3-$PM_{2.5}$ relationship over NYC and BJ (The blue shaded area indicates the range in the O_3-$PM_{2.5}$ slope, depending on the extent of SAP reductions. The DA24 $PM_{2.5}$ data were binned in increments of 5 μg m^{-3}.).

Figure 4. O_3 and $PM_{2.5}$, and related emissions in YRD and PRD. a, The O_3 vs $PM_{2.5}$ relationship of main urban cities in YRD for SP1 (2014-2016) and SP2 (2016-2019) (The error bar indicates 25-75% data range); **b,** The 2014 and 2016 MEIC anthropogenic emissions in YRD (including provinces of Shanghai, Jiangsu and Zhejiang); **c,** The O_3 vs $PM_{2.5}$ relationship of main urban cities in PRD for SP1 (2014-2016) and SP2 (2016-2019) (The error bar indicates 25-75% data range); **d,** The 2014 and 2016 MEIC anthropogenic emissions in PRD (including Guangzhou province).

FIGURES

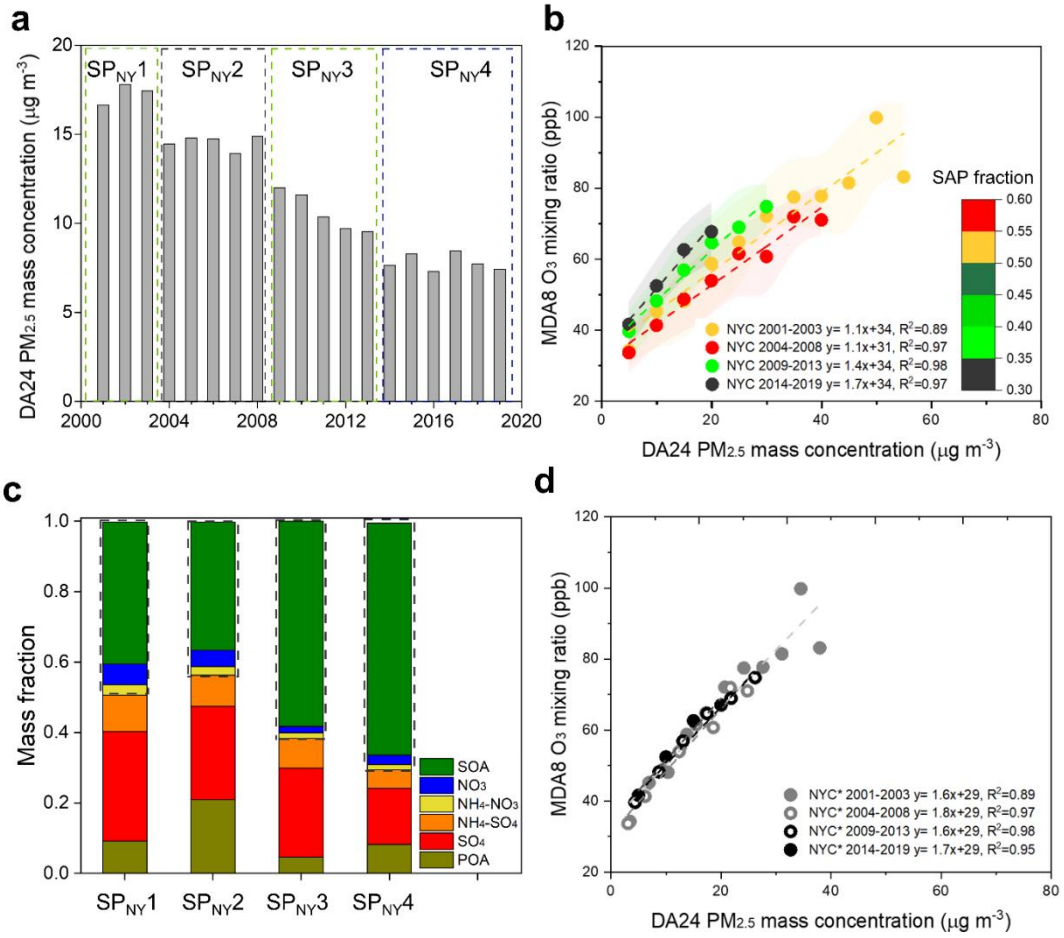

Figure 1. O_3 and $PM_{2.5}$ in NYC. a, The time series of the average DA24 $PM_{2.5}$ and top5% DA24 $PM_{2.5}$ mass concentrations in NYC for each subperiod specified in the main text (the dashed boxes indicate the four subperiods with subperiod 1 ($SP_{NY}1$): 2001-2003, subperiod 2 ($SP_{NY}2$): 2004-2008, subperiod 3 ($SP_{NY}3$): 2009-2013, subperiod 4 ($SP_{NY}4$): 2014-2019); **b,** NYC O_3-$PM_{2.5}$ relationship for the different subperiods (Colored by SAP mass fraction. The DA24 $PM_{2.5}$ data were binned in increments of 5 μg m^{-3}. The shaded area indicates 25%-75% data range of each bin. The O_3 concentration of each point was obtained by averaging the 25%-75% data. All p-value < 0.01); **c,** The aerosol mass fraction for each subperiod in NYC based on the AMS measurement from the representative year (2001 for $SP_{NY}1$, the average of 2001 and 2009 for $SP_{NY}2$, 2011 for $SP_{NY}3$ and 2018 for $SP_{NY}4$. Black dash box indicates non-SAP compounds, including SOA, nitrate and nitrate-related-ammonia); **d,** Adjusted O_3-$PM_{2.5}$ relationship when removing the influence of variability in SAP (* means adjusted value. All p-value < 0.01).

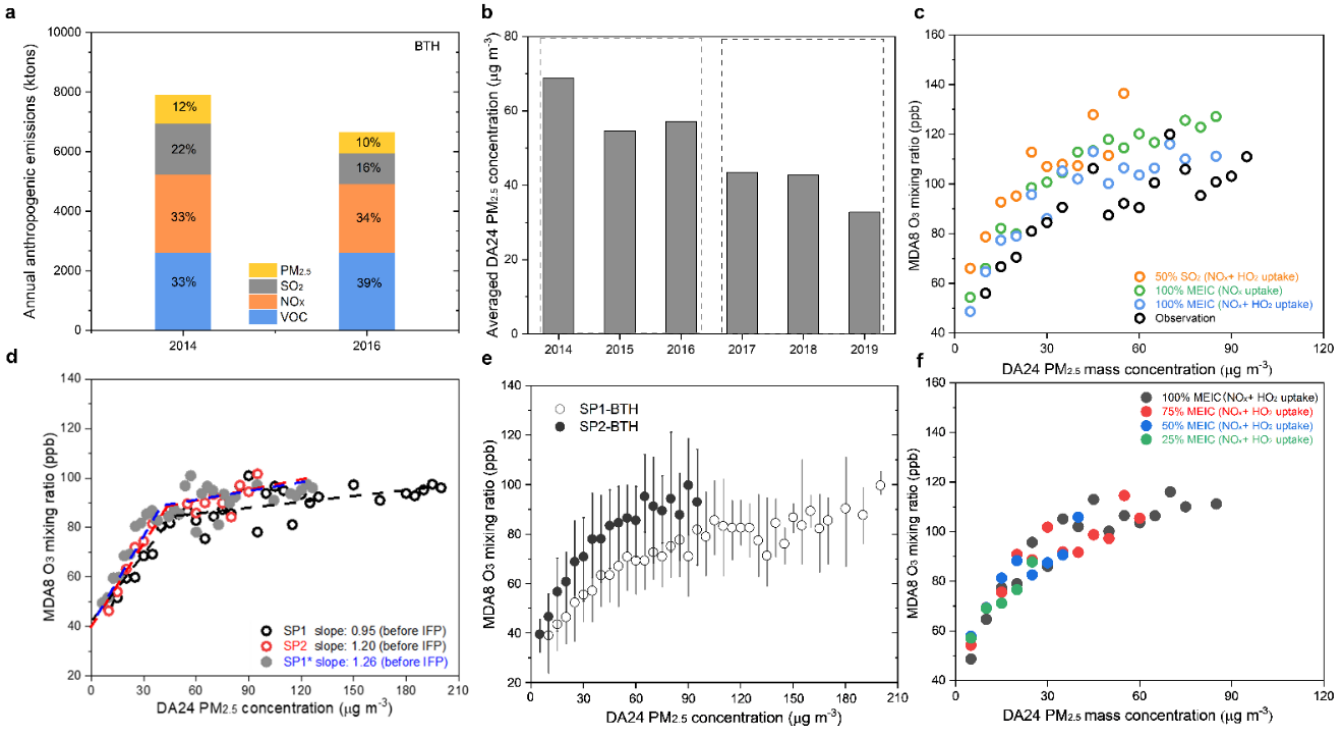

Figure 2. O_3 and $PM_{2.5}$, and related emissions in BJ and BTH. **a**, The 2014 and 2016 MEIC anthropogenic emissions in BTH (including provinces of Beijing, Tianjin and Hebei) (Note: 2016 MEIC anthropogenic emissions was used for 2017 summertime simulation and also for showing the emission variation trend); **b**, The time series of the average DA24 $PM_{2.5}$ and top5% DA24 $PM_{2.5}$ mass concentrations (the dash boxes indicate the two subperiods with subperiod 1 (SP1): 2014-2016, subperiod 2 (SP2): 2017-2019) ; **c**, The O_3 vs $PM_{2.5}$ relationship for observations, CMAQ simulations with only NOx uptake, CMAQ simulations with NOx and HO_2 uptake, and 50% abatements of SO_2 emissions for 2017; **d**, The O_3-$PM_{2.5}$ relationship of BJ for SP1 and SP2, and the adjusted O_3-$PM_{2.5}$ relationship based on the mass fraction in (c) (denoted by * in the legend, the $PM_{2.5}$ data were binned in increments of 5 μg m^{-3}) ; **e**, The O_3 vs $PM_{2.5}$ relationship of main urban cities in BTH for SP1 and SP2 (including Beijing, Tianjin, Shijiazhuang, Tangshan and Baoding, and the locations were shown in Fig. S5. The error bar indicates 25-75% data range); **f**, The O_3 vs $PM_{2.5}$ relationship for different simultaneous emission abatement scenarios based on CMAQ simulations with NOx and HO_2 uptake for 2017.

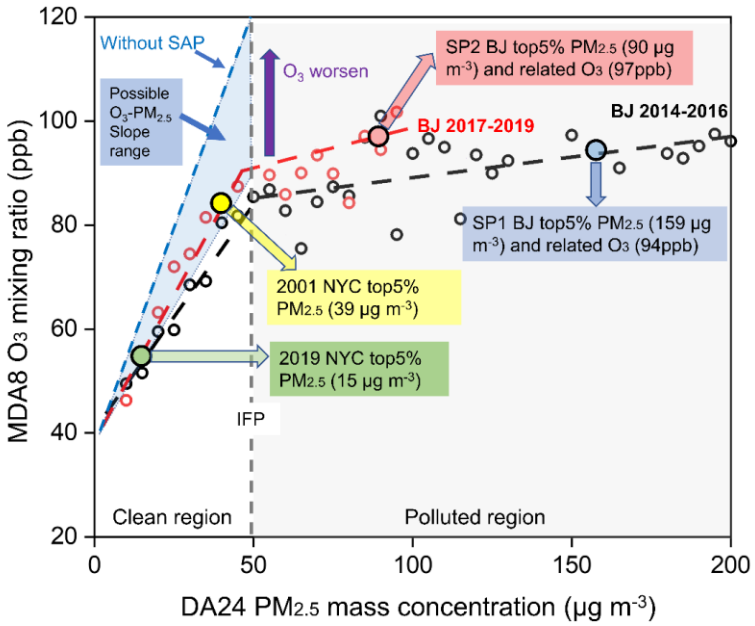

Figure 3. Diagram of the current and future O_3-$PM_{2.5}$ relationship over NYC and BJ (The blue shaded area indicates the range in the O_3-$PM_{2.5}$ slope, depending on the extent of SAP reductions. The DA24 $PM_{2.5}$ data were binned in increments of 5 μg m^{-3}.).

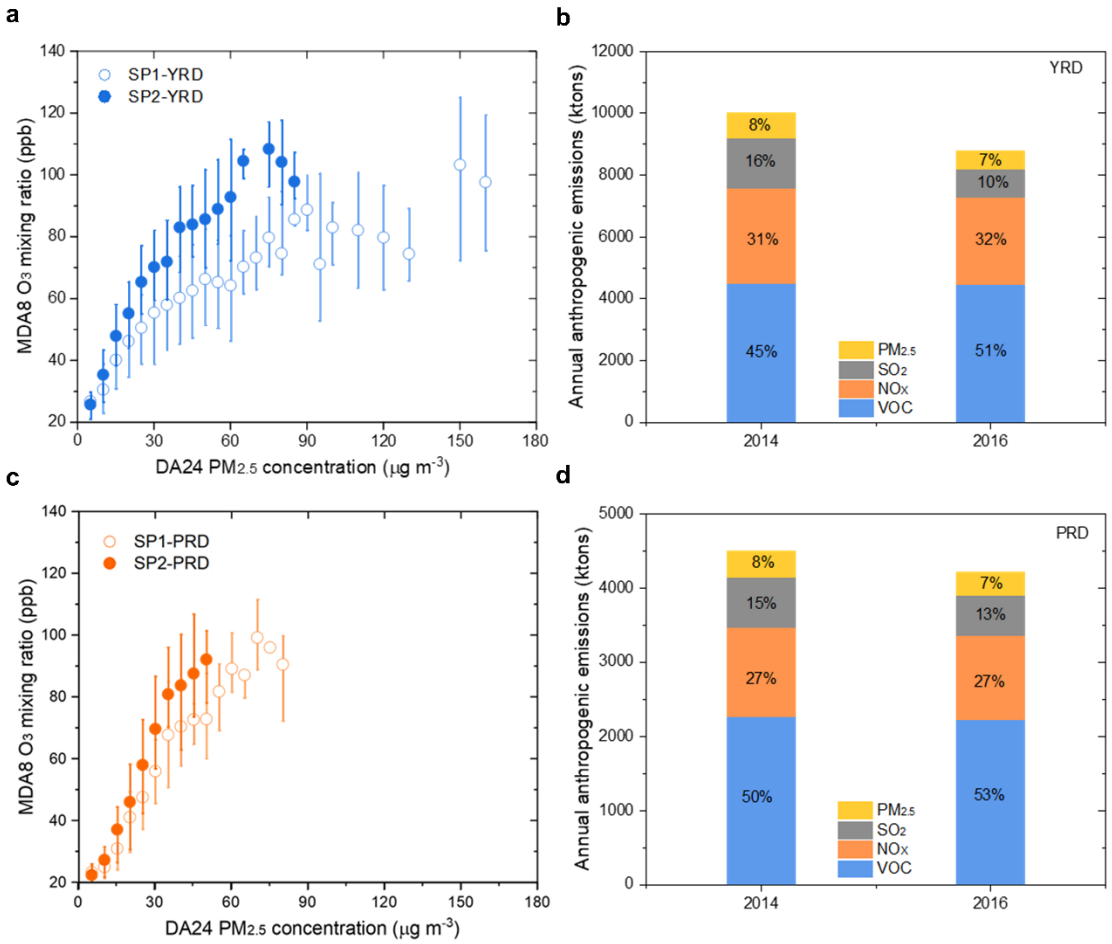

Figure 4. O_3 and $PM_{2.5}$, and related emissions in YRD and PRD. a, The O_3 vs $PM_{2.5}$ relationship of main urban cities in YRD for SP1 (2014-2016) and SP2 (2016-2019) (The error bar indicates 25-75% data range); **b,** The 2014 and 2016 MEIC anthropogenic emissions in YRD (including provinces of Shanghai, Jiangsu and Zhejiang); **c,** The O_3 vs $PM_{2.5}$ relationship of main urban cities in PRD for SP1 (2014-2016) and SP2 (2016-2019) (The error bar indicates 25-75% data range); **d,** The 2014 and 2016 MEIC anthropogenic emissions in PRD (including Guangdong province).